High-Fidelity CNOT Gate for Donor Electron Spin Qubits in Silicon

Ludwik Kranz,[1,2] Stephen Roche,[1] Samuel K. Gorman,[1,2] Joris. G. Keizer,[1,2] and
Michelle Y. Simmons[1,2,*]

[1]*Centre of Excellence for Quantum Computation and Communication Technology, School of Physics, University
of New South Wales, Sydney, New South Wales 2052, Australia*
[2]*Silicon Quantum Computing Pty Ltd., UNSW, Sydney, Australia*

Donor dots realized with phosphorus atoms in silicon have proven to be excellent hosts for electron spin qubits as they provide a strong confining potential that results in small wave functions and well-isolated ground states. As a promising candidate for large-scale quantum computers, such qubits have demonstrated fast, high-fidelity single-shot readout (99.8%) and extremely long coherence times (seconds) with single-qubit gates exceeding 99.94% fidelity. However, high-fidelity two-qubit gates in this platform have been elusive, with charge noise being one of the key limiting factors. Charge noise causes unwanted fluctuations in the exchange coupling between electron spins resulting in logic gate errors, a process that could be minimized if we could engineer a large enough magnetic field difference between the qubits. In this work, we show that using the donor nuclear spins as nanomagnets we can engineer a large magnetic field gradient (> 800 MHz) between the qubits thereby minimizing sensitivity to charge noise and reducing errors during two-qubit controlled-NOT (CNOT) gate operation. We develop a comprehensive theoretical framework with realistic noise sources for performing CNOT gates via controlled rotation (CROT) using multidonor dot qubits. We show that by engineering the number and location of donors within the dots we can control the hyperfine couplings to maximize the energy difference between electron spin qubits. As a result, we show that the CNOT gate error rates can be reduced by a factor of 4 when using multidonor dots as compared to single donors. Our results provide a theoretical roadmap to show how to achieve CNOT fidelities as high as 99.98% by optimizing both the local magnetic environment and the operating parameters of multidonor dot qubits.

I. INTRODUCTION

In 1998 Kane [1] proposed a quantum computing platform in silicon, where electron spin states are hosted on single phosphorus (P) donors. In Kane's original proposal, qubits were encoded into an array of the P donor nuclear spins with two-qubit gates performed via the exchange coupling, J, between electron spins hosted on adjacent P atoms. To achieve the required magnitude of J for a two-qubit gate, P atoms had to be placed in the silicon host crystal with nanometer precision [2–4]. 20 years after Kane's proposal, this challenge was recently met by He *et al.* [5] by exploiting the subnanometer precision of STM lithographic techniques [6] to demonstrate the first two-qubit gate between donor-bound electron spins in

silicon. The ability to perform two-qubit gates, combined with long (30 s) electron-spin lifetimes [7] and single-qubit gate fidelities in excess of 99.94% [8], establishes donor atom qubits in silicon as a competitive quantum computing platform for scaling.

The next key milestone for atom-based electron-spin qubits is improvement of two-qubit gate fidelities [5,9], which have yet to meet the 99% fidelity threshold required to build a large-scale error-corrected quantum computer [10]. To optimize two-qubit gate fidelities, it is worthwhile to consider three different types of gates that can be employed as native entangling gates between electron spins: SWAP$^\alpha$, controlled-phase (CPHASE), and controlled-rotation (CROT). The two-qubit SWAP$^\alpha$ gates, such as $\sqrt{\text{SWAP}}$ and SWAP, can be implemented in a straightforward way using a timed voltage pulse that swaps the antiparallel spin states $|\downarrow\uparrow\rangle$ and $|\uparrow\downarrow\rangle$ [5,11]. SWAP$^\alpha$ gates require large J, which allows for the gate to be completed in a short time (approximately 1 ns) [5,11]. At the same time, due to the large magnitude of J these gates are inherently sensitive to charge noise [12], which can hinder the two-qubit gate fidelities. The susceptibility to charge noise

---

*Corresponding author. michelle.simmons@unsw.edu.au

is reduced when using CPHASE and CROT gates. The CPHASE gate relies on a voltage pulse that introduces a phase difference between the $|\downarrow\uparrow\rangle$ and $|\uparrow\downarrow\rangle$ states [13–16]. When combined with single-qubit operations, the CPHASE gate can be used to execute the two-qubit CNOT gate [13,14], a maximally entangling two-qubit gate widely used in quantum computing algorithms and error correction [17]. The CROT gate, on the other hand, is a resonantly driven gate that relies on the control qubit governing the resonant energy of the target qubit [18–20]. Both CPHASE and CROT gates are operated in the regime where the J coupling is smaller than the energy difference ΔE between the two qubits. In this regime J is less sensitive to charge noise (compared to SWAP$^\alpha$ gates) [12,21], making both CROT and CPHASE promising candidates for achieving high fidelities. The CROT gate is particularly attractive due to its simplicity, since the CNOT gate can be directly implemented in a single step via an adequately timed CROT operation [18,19].

During the CNOT gate, the control qubit remains unchanged while the target qubit is flipped, for example from $|\downarrow\rangle$ to $|\uparrow\rangle$ state. Therefore, to achieve a high-fidelity CNOT gate via CROT, it is useful to engineer a large $\Delta E/J$ ratio such that both qubits remain in their computation eigenbases $\{|\downarrow\rangle, |\uparrow\rangle\}$ [19,22]. Additionally, the larger the $\Delta E/J$ ratio the weaker the sensitivity to charge noise during the exchange pulse [12]. For gate-defined silicon quantum dots, the large $\Delta E/J$ ratio is typically achieved by placing metallic micromagnets near the quantum dots to create a large magnetic field gradient between the qubits. While the addition of micromagnets helps maintain the qubits in their computational bases during two-qubit gates, these metallic structures can add extra charge noise as well as increase the sensitivity of the qubits to charge noise, reducing the qubit coherence time [14,23].

In this paper we present a strategy to achieve large magnetic field gradients ΔE between donor atom qubits, while preserving the inherently low-noise crystalline qubit environment of donor-based qubits [24]. To achieve this, we propose a CROT gate between electron spins hosted on multidonor dots where instead of using external magnets, we use the donor nuclear spins as atomic "magnets" to produce strong local magnetic fields at the qubit sites. When initialized in opposite directions, the nuclear spins on both dots can collectively create the large ΔE required for a high-fidelity CROT gate. As previously shown by Kalra *et al.* [22], for two-qubit gates between exchange-coupled pairs of *single* P atoms, ΔE is limited by the hyperfine coupling of a single donor to approximately 117 MHz, resulting in calculated theoretical CNOT gate fidelities exceeding 99.9% in isotopically purified ^{28}Si and in the absence of charge noise. Here, we extend this model to multidonor dots and we explain how the CNOT gate fidelities can be increased via atomic scale engineering by precisely controlling the spatial arrangement of donor

atoms. We find that, due to the strong hyperfine couplings, atomically engineered multidonor dot qubits are particularly well suited for CROT gates as they can produce large ΔE in excess of 800 MHz. In order to determine the impact that ΔE has on the CNOT fidelity, we construct a numerical model that includes the interplay between different CNOT gate error sources. Our model enables us to find the optimal experimental parameters, such as the drive frequency and the gate duration time, that maximize the CNOT gate fidelity. In addition, we expand on the previous two-qubit gate theory models by including charge noise, which is one of the main error sources for exchange-based two-qubit gates. Using a realistic nonlinear mapping of charge noise to exchange coupling [25] we can estimate the true impact of charge noise on CNOT gate fidelity. We find that due to the large ΔE of multidonor dots, the sensitivity to charge noise is reduced compared to single donors, and errors associated with departing from the computational two-qubit subspace are minimized. We show that for multidonor dot qubits the achievable CNOT fidelities depend not only on the number of P donors in each qubit but also the atomic configuration of the P atoms within each qubit, which highlights the benefit of atomic scale engineering. Of note, we find that assuming realistic levels of charge noise ($\sigma_\epsilon \simeq 2\,\mu$eV), atomically engineered multidonor dot qubits are capable of CNOT errors as low as 0.024%, well below the required 1% fault-tolerant threshold [17].

II. UTILIZING THE NUCLEAR SPINS AS ATOMIC MAGNETS

The energy difference ΔE between two qubits plays a crucial role during two-qubit gates. The strategies for achieving ΔE in silicon devices vary between different platforms as schematically presented in Fig. 1. For gate-defined quantum dots, formed at the Si/SiGe and Si/SiO$_2$ interfaces, the Zeeman splitting of each qubit is defined by the local magnetic field B_0 as well as the local electric field, which can also affect the electron g factor due to the Stark shift [26]. Figure 1(a) schematically shows a Si/SiGe device where the difference in qubit energies is achieved by placing qubits in a magnetic field gradient produced by a specially designed micromagnet [14,18,19]. The Si-MOS devices, on the other hand, typically utilize ΔE arising from the roughness of the Si/SiO$_2$ interface, which results in variations in the electron's g factor amongst different qubit sites [18] [see Fig. 1(b)].

In contrast, for donor-based qubits, the energy splitting E can be engineered by controlling the hyperfine coupling between the electron spin and the nuclear spin of the qubit-hosting phosphorus atom (or atoms). To illustrate an example of this, in Fig. 1(c) we schematically show two electron-spin qubits confined by two P donors (2P, left) and a single donor (1P, right). The magnitude of the hyperfine coupling A depends on the number of donors within a qubit
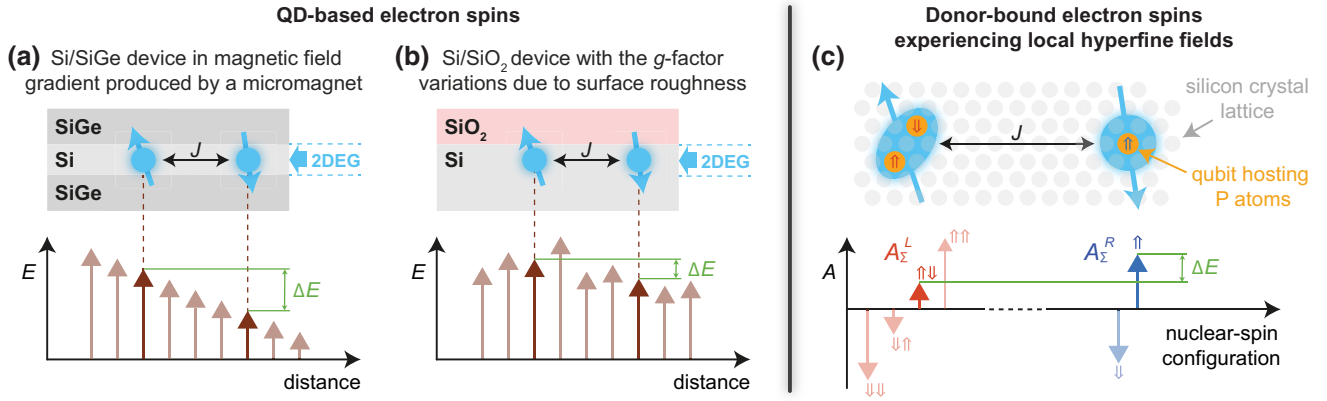
FIG. 1. Illustrative representation showing the origin of ΔE between electron-spin qubits hosted in different quantum dots (a),(b) and donors (c) in silicon. (a) The sketch shows two electron spins in quantum dots electrostatically defined within the two-dimensional electron gas (2DEG) at the interface between Si (light gray) and SiGe (dark gray). The lower panel shows the gradient in Zeeman energy as a function of distance, where ΔE between qubits arises due to the slanting magnetic field produced by a micromagnet typically placed on the surface of such Si/SiGe devices. (b) In Si-MOS devices, the 2DEG forms at the interface between Si and SiO$_2$, where the electron experiences spin-orbit-mediated variations in the g factor due to the atomic nonuniformities at the Si/SiO$_2$ interface. As a result, each qubit has a slightly different Zeeman energy, with ΔE on the order of approximately 10 MHz between neighboring dots [18]. (c) Schematic representation of an atomic-scale device where electrons are spatially bound to precision-placed donors in silicon. In the example shown here, the left electron is confined by a pair of closely placed P donors, and the right electron by a single donor. For atom qubits, the ΔE parameter is dominated by the local hyperfine fields due to the hyperfine interaction, A, between electron (light blue ovoids) and nuclear spins (double-lined arrows ⇓ and ⇑). Consequently, the temporal orientation of nuclear spins within both qubits defines the value of ΔE between them.

and their mutual atomic arrangement [27,28]. As a result, the qubit energy difference ΔE depends on

    (a) the number of donors in each dot,
    (b) the atomic arrangement of donors in each dot,
    (c) the orientation of P nuclear-spin states in each dot.

In this paper we discuss how each of these factors impacts the CNOT fidelity. It is worthwhile to realize that the first two factors (number and spatial location of donors) are established during the fabrication of the device, with the last factor (orientation of nuclear spins) dynamically controlled via nuclear magnetic resonance (NMR). Hence, the nuclear-spin initialization can be achieved via NMR by applying rf pulses that match the nuclear-spin energy splitting, as demonstrated for single donors [29,30] and recently also for multidonor dots [31]. In the following sections we explain how to initialize nuclear spins via NMR such that the CNOT fidelity is maximized.

III. OPERATION OF A CROT GATE

The two-qubit CROT gate requires both electric and magnetic control. The magnetic control, needed to drive the individual electron spins, can be achieved using electron-spin resonance (ESR) techniques [32]. The electric control, necessary to control the J coupling, can be implemented by applying voltages to in-plane control gates that can tune the relative energy levels of the two qubits [5,33]. Due to the J coupling, the ESR transition of each qubit is dependent on the state of the other qubit, which is the basis of the CROT gate. To illustrate this, in Fig. 2(a) we show a schematic energy diagram of a two-electron-spin system as a function of detuning energy, ϵ, where $\bar{E}$ is the average Zeeman splitting of the qubit pair and ΔE is the energy difference between qubits. The left-hand side of the energy diagram corresponds to the isolated spin basis $\{|\downarrow\downarrow\rangle, |\downarrow\uparrow\rangle, |\uparrow\downarrow\rangle, |\uparrow\uparrow\rangle\}$, where the red and blue arrows correspond to the ESR transitions of the left and right qubit, respectively. As the detuning, ϵ, is increased, the exchange coupling changes the transition energy f^L (f^R) of the left (right) qubit by $\pm J/2$ (energy shift can be positive or negative depending on the spin orientation of the other qubit). The right-hand side of the diagram in Fig. 2(a) corresponds to the hybridized basis of the spin states $\{|\downarrow\downarrow\rangle, |\widetilde{\downarrow\uparrow}\rangle, |\widetilde{\uparrow\downarrow}\rangle, |\uparrow\uparrow\rangle\}$, where the tilde indicates the hybridization of the antiparallel states, $|\downarrow\uparrow\rangle, |\uparrow\downarrow\rangle$, due to finite exchange energy J [19].

During a CROT operation, a timed ESR pulse rotates the target qubit, under the condition that the control qubit is in a $|\uparrow\rangle$ state [14,19]. Throughout this work we arbitrarily select the left (right) qubit to be the target (control) qubit, so that the ESR pulse applied at frequency $f^L_\uparrow = f^L + J/2$ will rotate the left qubit (target) only if the right qubit
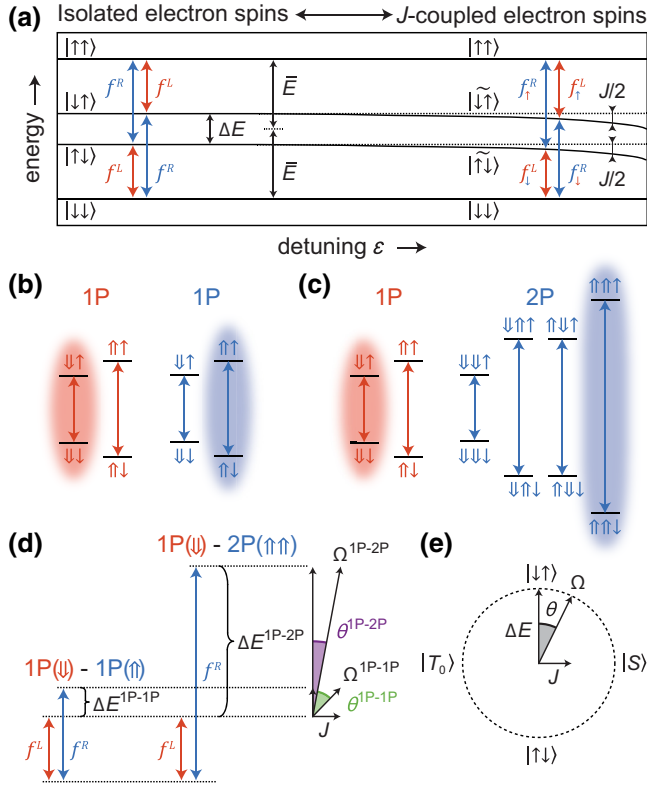
FIG. 2. Using multidonor qubits to create large qubit energy difference ΔE. (a) Energy diagram of a two-electron system. Red (blue) arrows represent ESR transitions f^L (f^R) of left (right) electron. At large negative detunings (left side), the electrons are well separated and the exchange interaction, J is small. As the detuning ϵ is increased (right side), J detunes the qubits' transition energies, depending on the spin of the second electron. (b),(c) Energy-level diagrams of 1P-1P and 1P-2P qubit pairs. Single ($\downarrow / \uparrow$) and double ($\Downarrow / \Uparrow$) arrows represent electron and nuclear-spin states, respectively. For clarity, the left qubits are shown in red and right qubits in blue. For each qubit pair, highlighted with the colored ovals we show the antiparallel nuclear-spin configurations that provide the largest possible difference in transition energies between the two qubits. To maximize the fidelity of the CNOT gate, the nuclear spins should be initialized in such an antiparallel configuration, that is $|\Downarrow \cdot \Uparrow\rangle$ for 1P-1P and $|\Downarrow \cdot \Uparrow\Uparrow\rangle$ for 1P-2P. (d) The transition energy difference ΔE between two qubits is larger for 1P-2P compared to 1P-1P. As a result, the angle $\theta = \arctan(J/\Delta E)$ for exchange-coupled 1P-2P qubits is smaller than in the case of 1P-1P qubits. (e) A schematic representation of the Bloch sphere of the two electron-spin system. Since the qubits are measured in the single spin basis, any deviation from the vertical $|\downarrow\uparrow\rangle/|\uparrow\downarrow\rangle$ axis results in state leakage into the singlet-triplet ($S - T_0$) basis. Since the 1P-2P qubit pair provides a smaller angle θ, the leakage error during the CNOT gate is reduced.

(control) is in the $|\uparrow\rangle$ state. The CNOT gate is achieved when the controlled rotation angle is exactly π [19]. After the controlled rotation, both qubits are independently measured via a projective spin readout [11].

The CROT gate requires that J is much smaller than ΔE, so that the two-electron-spin system remains in the computational eigenbasis, and is therefore less sensitive to charge noise [14,19,21,22]. Hence, to achieve a high-fidelity CROT gate, it is desirable to engineer a large ΔE [18,19]. We show how we can achieve large ΔE using multidonor qubit pairs, such as 1P-2P, 1P-3P, or 2P-3P, where the P nuclear spins can be used as atomic "magnets" to create a large ΔE, exceeding 800 MHz, thus mitigating the need to either integrate micromagnets on the devices or engineer the spin-orbit coupling.

IV. USING MULTIDONOR QUBITS TO REDUCE SENSITIVITY TO CHARGE NOISE

To illustrate the benefit of multidonor qubits, in Figs. 2(b) and 2(c) we compare the energy-level diagrams between the 1P-1P and 1P-2P qubit pairs along with their ESR transitions marked by vertical double-headed arrows. The ESR transitions of the left (right) qubit are indicated with a red (blue) color. Each ESR transition corresponds to a specific configuration of the nuclear-spin states, with two possible configurations for a 1P qubit, $|\Downarrow\rangle$ and $|\Uparrow\rangle$, and four configurations for a 2P qubit, $|\Downarrow\Downarrow\rangle$, $|\Downarrow\Uparrow\rangle$, $|\Uparrow\Downarrow\rangle$, and $|\Uparrow\Uparrow\rangle$. Prior to executing a CNOT gate, the nuclear spins of the P donors within the dots must be initialized via NMR so that the qubit transition energies are known and fixed throughout the CNOT gate operation. For the CNOT gate, it is beneficial to orientate the donor nuclear spins in one donor dot such that they are antiparallel to the nuclear spins in the other donor dot. For example, all P nuclear spins in the left qubit pointing down and all P nuclear spins in the right qubit pointing up. Such antiparallel nuclear-spin configurations are highlighted with the colored ovals in Figs. 2(b) and 2(c). Next, in Fig. 2(d) we compare the ΔE values that arise from these antiparallel nuclear spin configurations for 1P-1P and 1P-2P qubit pairs. The qubit energy difference, ΔE, is much larger for 1P-2P than for 1P-1P due to the stronger electron confinement, and hence larger A, of the 2P qubit [27,28].

Large values of ΔE are desirable for a two-qubit CROT gate as they help retain qubits in the their computational basis, where errors associated with charge noise are minimized. The advantage of a large ΔE value is schematically shown in Figs. 2(d) and 2(e). During the controlled rotation of the target qubit, the two-electron-spin system is in the hybridized basis $\{|\downarrow\downarrow\rangle, |\widetilde{\downarrow\uparrow}\rangle, |\widetilde{\uparrow\downarrow}\rangle, |\uparrow\uparrow\rangle\}$, where the effective coupling between the $|\widetilde{\downarrow\uparrow}\rangle$ and $|\widetilde{\uparrow\downarrow}\rangle$ corresponds to [5],

$$\Omega = \sqrt{\Delta E^2 + J^2}. \tag{1}$$

As schematically presented on the Bloch sphere in Fig. 2(e), the hybridization of the antiparallel states can be quantified using the angle $\theta = \arctan(J/\Delta E)$ that defines

the two-qubit basis as follows [18,19]:

$$|\widetilde{\uparrow\downarrow}\rangle = -\sin\left(\frac{\theta}{2}\right)|\downarrow\uparrow\rangle + \cos\left(\frac{\theta}{2}\right)|\uparrow\downarrow\rangle, \qquad (2)$$

$$|\widetilde{\downarrow\uparrow}\rangle = \cos\left(\frac{\theta}{2}\right)|\downarrow\uparrow\rangle + \sin\left(\frac{\theta}{2}\right)|\uparrow\downarrow\rangle, \qquad (3)$$

where

$$\sin\left(\frac{\theta}{2}\right) = \frac{J}{\sqrt{\left(\Delta E + \sqrt{\Delta E^2 + J^2}\right)^2 + J^2}}, \qquad (4)$$

$$\cos\left(\frac{\theta}{2}\right) = \frac{\Delta E + \sqrt{\Delta E^2 + J^2}}{\sqrt{\left(\Delta E + \sqrt{\Delta E^2 + J^2}\right)^2 + J^2}}. \qquad (5)$$

The angle θ determines the level of hybridization during the exchange pulse, and hence the sensitivity to charge noise. The overall energy fluctuations between the hybridized states, $|\widetilde{\downarrow\uparrow}\rangle$ and $|\widetilde{\uparrow\downarrow}\rangle$, can be approximated as [21],

$$\delta_\Omega = \delta_B \frac{\partial\Omega}{\partial(\Delta E)} + \delta_\epsilon \frac{\partial J}{\partial\epsilon} \times \frac{\partial\Omega}{\partial J}, \qquad (6)$$

where δ_B is magnetic noise affecting the qubit energy difference ΔE, and δ_ϵ corresponds to charge-noise-induced detuning fluctuations that impact exchange coupling J. Consequently, large $\Delta E/J$ ratio reduces the sensitivity of Ω to charge noise $\partial\Omega/\partial J$. As shown in Fig. 2(d), the 1P-2P qubit pair provides a larger ΔE and smaller θ as compared to single donors (1P-1P). This means that for a given value of J, sensitivity to charge noise is much smaller for a 1P-2P compared to 1P-1P. To quantify the impact of donor numbers on the two-qubit gate fidelity, in the following sections we use a theoretical model to calculate the CROT gate fidelities for multidonor qubits.

V. THEORY MODEL

The previous section shows that due to their large ΔE values multidonor qubit pairs promise reduced errors from charge noise and increased CNOT gate fidelities. In order to quantify the impact of ΔE on the CNOT gate fidelity, we construct a numerical model based on the time evolution of the two-electron-spin Hamiltonian [22,34],

$$H = \overbrace{\gamma_e B_0(S_z^L + S_z^R)}^{H_Z} + \overbrace{\sum_{j=1}^{N_L} A_j^L \mathbf{S^L}\cdot\mathbf{I_j^L} + \sum_{k=1}^{N_R} A_k^R \mathbf{S^R}\cdot\mathbf{I_k^R}}^{H_A}$$

$$+ \overbrace{J(\mathbf{S^L}\cdot\mathbf{S^R})}^{H_J}, \qquad (7)$$

where γ_e is electron gyromagnetic ratio [32], B_0 is the global magnetic field strength, **S** and **I** are electron and

nuclear spin operators, N_L (N_R) is a number of donors within the left (right) qubit, A_i is the hyperfine strength between an electron and an individual donor site i, and the H_Z, H_A, and H_J parts of the Hamiltonian correspond to Zeeman, hyperfine and exchange contributions, respectively. The nuclear Zeeman energy of donor dots has been neglected as it is much smaller (approximately 20 MHz) than both the electron Zeeman energy (approximately 40 GHz) and the hyperfine energy (typically hundreds of MHz) [22]. To drive the ESR transitions of donor qubits, we consider an oscillating magnetic field $B_{ac}(t)$ perpendicular to B_0. Using this rotating frame approximation, in the absence of exchange interaction the total two-electron-spin Hamiltonian can be diagonalized and written in the $\{|\downarrow\downarrow\rangle, |\downarrow\uparrow\rangle, |\uparrow\downarrow\rangle, |\uparrow\uparrow\rangle\}$ eigenbasis as [18,22,35]

$$H_{RF} = \frac{1}{2}\begin{pmatrix} 2\bar{E} & \gamma_e B_1 & \gamma_e B_1 & 0 \\ \gamma_e B_1 & -\Delta E & 0 & \gamma_e B_1 \\ \gamma_e B_1 & 0 & \Delta E & \gamma_e B_1 \\ 0 & \gamma_e B_1 & \gamma_e B_1 & -2\bar{E} \end{pmatrix}, \qquad (8)$$

where $B_1 = B_{ac}/2$. The energy difference, ΔE, between qubits L and R can be written as

$$\Delta E = \left| E^L - E^R \right| \approx \left| \sum_{i=1}^{N_L} \langle I_z\rangle_i A_i^L - \sum_{j=1}^{N_R} \langle I_z\rangle_j A_j^R \right|, \qquad (9)$$

and the mean qubit energy, $\bar{E}$, as

$$\bar{E} = \frac{E^L + E^R}{2} \approx \gamma_e B_0 + \frac{1}{2}\left(\sum_{i=1}^{N_L} \langle I_z\rangle_i A_i^L + \sum_{j=1}^{N_R} \langle I_z\rangle_j A_j^R \right), \qquad (10)$$

where $\langle I_z\rangle_k = \pm\frac{1}{2}$ is the expectation value of the nuclear spin operator of the kth donor. In the presence of a finite J coupling between the qubits, the eigenbasis is changed to $\{|\downarrow\downarrow\rangle, |\widetilde{\downarrow\uparrow}\rangle, |\widetilde{\uparrow\downarrow}\rangle, |\uparrow\uparrow\rangle\}$ and the corresponding Hamiltonian can be written as

$$H_{RF}^J = \frac{1}{2}\begin{pmatrix} 2\bar{E} & \gamma_S B_1 & \gamma_T B_1 & 0 \\ \gamma_S B_1 & -\Omega - J & 0 & \gamma_S B_1 \\ \gamma_T B_1 & 0 & \Omega - J & \gamma_T B_1 \\ 0 & \gamma_S B_1 & \gamma_T B_1 & -2\bar{E} \end{pmatrix}, \qquad (11)$$

where γ_S and γ_T are the effective gyromagnetic ratios associated with singlet and triplet states, and can be expressed as

$$\gamma_S = \gamma_e\left[\cos\left(\frac{\theta}{2}\right) - \sin\left(\frac{\theta}{2}\right)\right], \qquad (12)$$

$$\gamma_T = \gamma_e\left[\cos\left(\frac{\theta}{2}\right) + \sin\left(\frac{\theta}{2}\right)\right]. \qquad (13)$$

We can now use the time evolution of the Hamiltonian H_{RF}^J to describe the two-qubit CROT operation between two exchange-coupled electron spins.

VI. CALCULATION OF CNOT GATE FIDELITY USING 1P-1P AND 1P-2P QUBITS

Using the theoretical framework outlined in the previous section, we calculate the CNOT fidelities achievable with 1P-1P and 1P-2P qubit pairs. We begin by calculating the ESR transition energies as a function of detuning for the 1P-1P qubit pair in Fig. 3(a) and for 1P-2P in Fig. 3(b). For the calculation of ΔE values, we use Eq. (9) and assume the hyperfine value of $A = 117$ MHz for the 1P qubit, which corresponds to the average bulk value of a single P donor in silicon [36], and $A = 366$ MHz for the 2P qubit, which corresponds to 0.384-nm separation between the 2P atoms [28]. We also assume that the nuclear spins in the two qubits are prepared in the antiparallel orientation in order to maximize ΔE. Such an antiparallel configuration yields $\Delta E = 117$ MHz for the 1P-1P qubit pair and $\Delta E = 425$ MHz for 1P-2P. For both qubit pairs, the exchange energy $J(\epsilon, t_c)$ is calculated using the Hubbard model [37–40],

$$J(\epsilon, t_c) = \frac{\epsilon}{2} + \sqrt{\frac{\epsilon^2}{4} + t_c^2}, \qquad (14)$$

with the tunnel coupling of $t_c = 4$ GHz, allowing for the exchange interaction J to be controllably switched *on* and *off* using electrostatic gates [5,33]. It has been experimentally shown that the tunnel coupling of $t_c = 4$ GHz corresponds to the two qubits being separated by a distance of approximately 13 nm [5]. As the detuning, ϵ, is increased, the ESR spectral line of the left (right) qubit is split into two lines that correspond to $|\downarrow\rangle$ and $|\uparrow\rangle$ spin states of the right (left) qubit, which can be written as

$$f^R_{\uparrow} = \bar{E} + \frac{1}{2}\left(\sqrt{\Delta E^2 + J^2} + J\right),$$

$$f^R_{\downarrow} = \bar{E} + \frac{1}{2}\left(\sqrt{\Delta E^2 + J^2} - J\right),$$

$$f^L_{\uparrow} = \bar{E} + \frac{1}{2}\left(-\sqrt{\Delta E^2 + J^2} + J\right),$$

$$f^L_{\downarrow} = \bar{E} + \frac{1}{2}\left(-\sqrt{\Delta E^2 + J^2} - J\right).$$

Having determined the ESR spectra of exchange-coupled 1P-1P and 1P-2P qubit pairs, we now calculate the corresponding CNOT gate fidelities. To achieve this, we calculate the unitary of the time evolution of our two-electron-spin system Hamiltonian H_{RF}^J [Eq. (11)]. The unitary operator is then used to calculate the process tomography matrix χ, which allows the process fidelity to be calculated

as $F = \text{Tr}(\chi^T \chi_{\text{ideal}})$, where χ_{ideal} is the ideal CNOT process matrix [41]. The ideal CNOT process matrix includes phase accumulations for each state, which can be corrected for using single-qubit rotations and a refocusing pulse sequence [18,20,22,42]. To account for decoherence during the CNOT gate, we consider Gaussian distributions with standard deviation σ_ϵ and σ_B that correspond to charge noise and magnetic noise, respectively. The CNOT fidelity is then calculated by sampling five values from each distribution and averaging over the corresponding time evolutions. Using the inverse transform sampling method [43] we find that five samples from a Gaussian distribution is sufficient to accurately calculate the CNOT gate fidelity. In our simulations we consider charge noise of $\sigma_\epsilon = 2$ μeV, as reported for state-of-the-art silicon qubits [24,44], and a magnetic noise of $\sigma_B = 2$ kHz corresponding to isotopically purified silicon ^{28}Si with a residual ^{29}Si concentration of 800 ppm [30]. For the microwave ESR pulses, we consider a square-shaped envelope of the oscillating ESR magnetic field, which allows for faster Rabi oscillations as compared to other pulse shapes (e.g., Gaussian) with the same power [22]. The exchange interaction is considered to be applied with a detuning pulse, where the duration of the exchange pulse is adjusted such that unwanted phase accumulations cancel each other out [20,42]. In addition, we assume that initialization of nuclear spins has negligible errors, as single-qubit gates with 99.99% fidelity have been reported for P nuclear spins in silicon [45]. It is also assumed that the desired antiparallel orientation of the nuclear spins is preserved throughout the experiment. This assumption is justified with the fact that the relaxation times of nuclear spins ($\gtrsim$ few mins) [29,30] are much longer than the typical CNOT gate operation time (< 10 μs) [14,19].

We now use our theoretical model to compare the CNOT fidelities achievable with 1P-1P and 1P-2P qubit pairs. Figures 3(c) and 3(d) show the calculated CNOT gate error as a function of applied ESR frequency and detuning for 1P-1P (c) and 1P-2P (d). The gate time T_{CNOT} has been set to 2 μs, which results in the highest fidelity as explained later in this work. It is worthwhile to note that for a given qubit pair, the optimal operating point is determined by the competition between different error sources (see Appendix A for more details on error sources). The dark-colored lines in Figs. 3(c) and 3(d) correspond to frequency $f^L_{\uparrow}$ at which the CROT gate is performed. Our model enables us to find the point in the ESR frequency/detuning space for which the total CNOT error is minimized. For the 1P-1P system, the lowest error of 0.096% is found for $f^L_{\uparrow} = \gamma_e B_0 - 56.1$ MHz and $\epsilon = -13.3$ meV. Similarly, for the 1P-2P system we find the optimal operating point for $f^L_{\uparrow} = \gamma_e B_0 - 54.3$ MHz and $\epsilon = -7.8$ meV with only 0.034% error. Our results show that the average CNOT error is three times smaller when using 1P-2P donor dots compared to single donors. This dramatic improvement
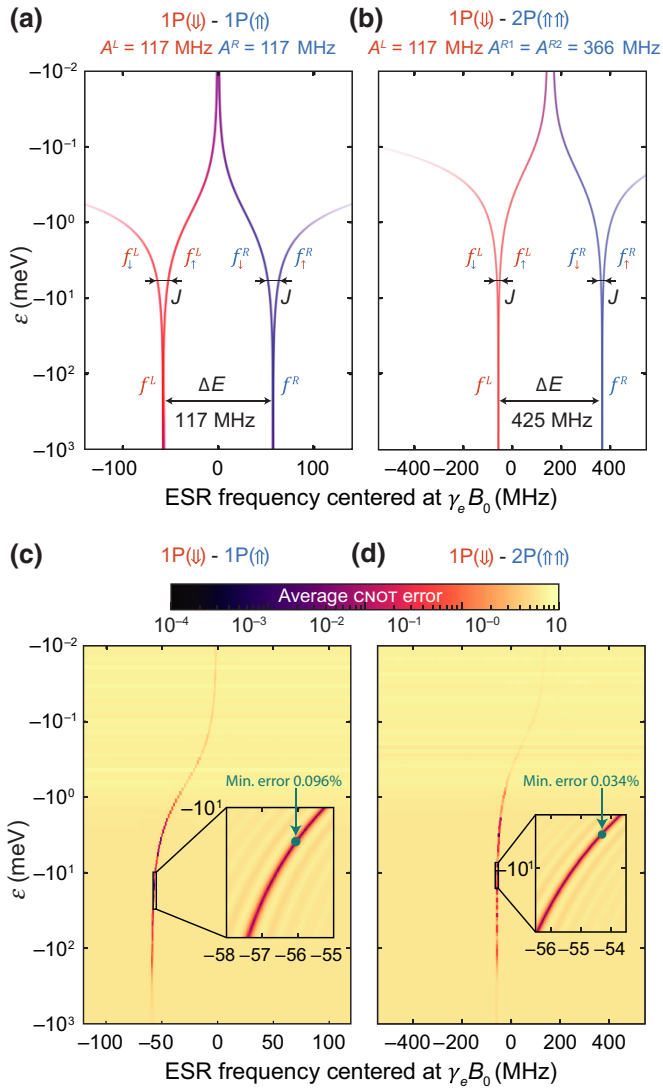
FIG. 3. CNOT gate based on a 1P-2P configuration yields 3 times smaller error compared to 1P-1P. (a) The ESR spectra of a 1P-1P qubit pair with the left qubit nuclear spin initialized in a $|\Downarrow\rangle$ state and the right qubit in a $|\Uparrow\rangle$ state. Such an antiparallel configuration yields a hyperfine energy difference of $\Delta E = 117$ MHz. The exchange coupling splits the spectral ESR line of each qubit into two branches, separated in energy by J. (b) Same as in (a) but for a 1P-2P qubit pair with nuclear states initialized in an antiparallel $|\Downarrow \cdot \Uparrow\Uparrow\rangle$ configuration that yields $\Delta E = 425$ MHz. (c) The CNOT gate error plotted as a function of detuning and ESR frequency for a 1P-1P qubit pair. Our model allows us to optimize the performance of a CNOT gate by finding the optimal exchange energy and the corresponding ESR frequency of the target qubit. For 1P-1P we find the lowest CNOT error of 0.096% for $f_\uparrow^L = \gamma_e B_0$ - 56.1 MHz and $\epsilon = -13.3$ meV. (d) Same as in (c) but for a 1P-2P qubit pair, with minimum error of 0.034%, a factor of 3 lower as compared to CNOT gate with 1P-1P. Here, the maximum fidelity is found for $f_\uparrow^L = \gamma_e B_0 - 54.3$ MHz and $\epsilon = -7.8$ meV. For both cases, (c) and (d), we assume magnetic Overhauser noise level of $\sigma_B = 2$ kHz corresponding to purified silicon (800 ppm ^{29}Si) [30], and charge-noise level of $\sigma_\epsilon = 2~\mu$eV [24].

can be attributed to the strong confining potential of the 2P donor dot that allows for an increased magnitude of ΔE.

VII. CNOT GATE WITH ATOMICALLY ENGINEERED DONOR DOTS

Having shown a threefold decrease in gate infidelity between 1P-1P and 1P-2P systems, we now investigate if the fidelity can be increased further using donor dots that contain even more P atoms. We primarily focus on the asymmetric pairs of multidonor dots (1P-2P, 1P-3P, and 2P-3P), which allow for a high level of tunability over the exchange coupling [46]. The CROT gate can be, in principle, executed between electron spins hosted by any arbitrary number of donors. However, the process of initializing all of the individual nuclear spins will likely become increasingly more challenging for excessive numbers of P atoms within qubits. Therefore, in this work we limit our considerations to qubit pairs containing no more than five donors in total (2P-3P). To begin, we consider the span of possible hyperfine values for 1P, 2P, and 3P qubits, as shown in Fig. 4(a). For each electron-spin qubit hosted by N P atoms, we calculate the total hyperfine,

$$A_\Sigma = \sum_{i=1}^{N} A_i. \qquad (15)$$

The A value of 1P is nominally fixed at 117 MHz; however, we note that this value can be slightly reduced in the presence of electric fields due to the Stark shift effect [28,47–49]. Unlike 1P, the 2P and 3P qubits do not have a fixed hyperfine value. Instead, A has been shown to depend on the exact crystallographic configurations of P atoms defining each qubit [27,28]. When the donors within the dot are close together, they form a strong confining potential, as the electron is more tightly bound, which results in higher A. Similarly, low A values correspond to larger interdonor separations within the dot, where the electron wave function is, on average, further away from each P atom. Consequently, depending on the crystallographic alignment of P atoms, A_Σ can take values between 120 and 732 MHz for the 2P qubit, and a range of 258–1050 MHz for the 3P qubit. The hyperfine values are obtained from tight binding numerical calculations in Refs. [27,28,48,50], which consider qubit donor arrangements up to eight lattice sites in the [110] crystallographic direction and two sites in the [1$\bar{1}$0] direction. Figure 4(a) shows several examples of different donor configurations for the 2P and 3P qubits with the corresponding ranges of A_Σ values.

Next, we determine the CNOT fidelities that can be achieved with different qubit pairs, 1P-1P, 1P-2P, 1P-3P, and 2P-3P. Figure 4(b) shows the average CNOT gate error as a function of ΔE [calculated using Eq. (9)] and gate time T_{CNOT}. The errors are calculated at the optimal detuning and ESR frequency, which means that for each point we
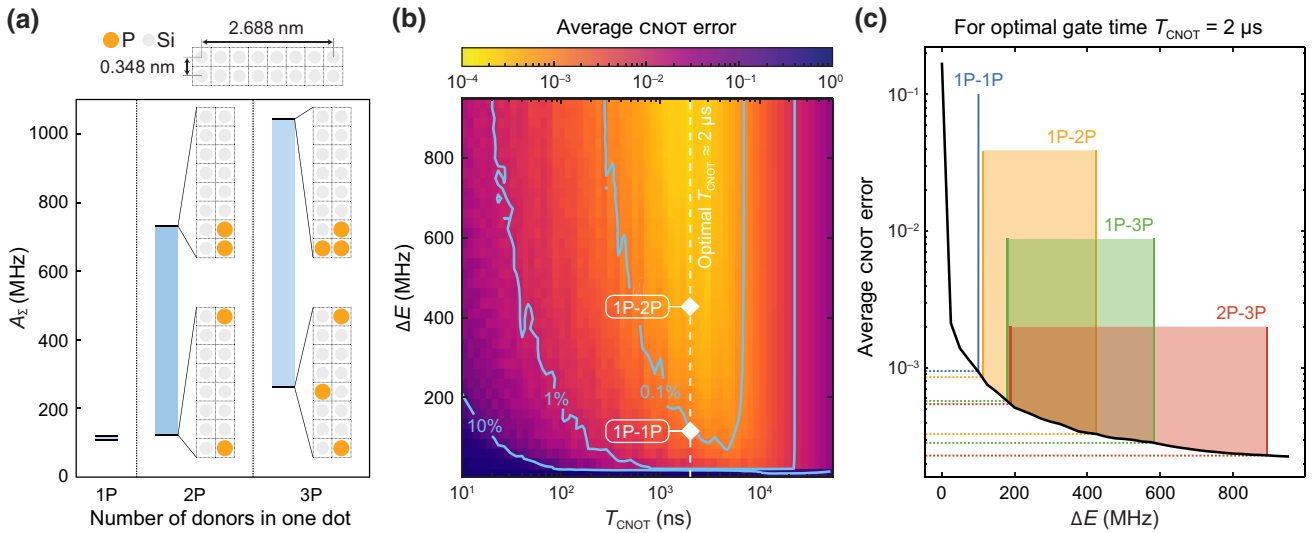
FIG. 4. Impact of the atomic qubit arrangements on the CNOT gate fidelity. (a) The range (shaded blue regions) of the hyperfine energies A_Σ for donor dots with 1, 2, and 3 phosphorus donor atoms. While the hyperfine value of a 1P is in principle fixed (117 MHz), the multidonor dots have a range of hyperfine values they can take, depending on the exact donor configuration within the silicon crystal lattice. The insets show the orientation of P atoms in the silicon crystal that correspond to the lowest and highest hyperfine values. In all cases, the donors are separated by less than 3 nm. The resultant A_Σ values, calculated as a sum of individual A couplings (per electron), range from 120 to 732 MHz for the 2P and from 258 to 1050 MHz for the 3P. (b) The CNOT gate error shown as a function of ΔE and the CNOT gate time T_{CNOT}. The white dashed line estimates the optimal two-qubit gate time of approximately 2 μs. (c) Performance of the CNOT gate for qubit pairs with different donor numbers. The black line shows the dependence between the CNOT error and the ΔE value, calculated for the optimal gate time of $T_{\text{CNOT}} \approx 2$ μs. The colored regions indicate the ΔE values achievable with different qubit pairs, based on the A_Σ ranges shown in (a). The dashed lines indicate the corresponding CNOT errors that can be achieved using different qubit pairs. The smallest error is found for qubit pairs that contain more donors, such as 2P-3P, as each donor nuclear spin can be used to increase ΔE thereby reducing the quantum state leakage.

generate a plot as in Figs. 3(c) and 3(d) and determine the minimum error value. The diamond markers in Fig. 4(b) correspond to the plots in Figs. 3(c) and 3(d) for 1P-1P and 1P-2P qubit pairs. For the noise levels considered (magnetic noise $\sigma_B = 2$ kHz and charge noise $\sigma_\epsilon = 2$ μeV), we find an optimal CNOT gate time at approximately 2 μs, as indicated with the dashed line in Fig. 4(b). This optimal CNOT gate time arises due to the interplay between two separate mechanisms. Fast CNOT gates (short T_{CNOT} times) correspond to increased driving power and broad excitation profiles in the frequency domain, which can effectively lead to the unwanted driving of the transitions $f_\downarrow^L$ and $f_\downarrow^R$, reducing the overall gate fidelity. Slow CNOT gates, on the other hand, suffer from the Overhauser dephasing as the resonant frequency of the target qubit fluctuates with the ^{29}Si nuclear bath. The competition between these two mechanisms sets an optimal gate time around $T_{\text{CNOT}} \sim 2$ μs [22] (for 800 ppm ^{29}Si), regardless of the qubit donor numbers.

Assuming the optimal gate time ($T_{\text{CNOT}} \sim 2$ μs), in Fig. 4(c) we show the minimum CNOT error achievable for a given value of ΔE. Based on the previously determined A_Σ values for individual qubits, we use Eq. (9) to find the ΔE values obtainable with different qubit pairs:

$\lesssim 117$ MHz for a 1P-1P, between 119 and 425 MHz for a 1P-2P qubit pair, 188–584 MHz for 1P-3P, and 189–891 MHz for 2P-3P. These ranges of ΔE values are indicated in Fig. 4(c), with the corresponding CNOT errors indicated with dashed lines. It is desirable for the ΔE values to be as high as possible since they correspond to the highest achievable CNOT fidelities.

The most advantageous ΔE values can be realized via atomic scale engineering, where the P atoms are placed close to each other in the silicon crystal lattice with atomic precision [see the upper graphics in Fig. 4(a)]. To date, the incorporation of P atoms into the silicon crystal lattice has a placement accuracy of approximately ± 1 lattice site due to the dissociative chemical processes that take place during the incorporation pathway [6]. As shown in Fig. 4(c), we find that the asymmetric qubit pairs 1P-2P, 1P-3P, and 2P-3P outperform two single donors, regardless of the atomic configurations of the multidonor qubits. Therefore, with the existing ± 1 lattice-site accuracy, it remains beneficial to use multidonor qubits since they allow for high CNOT fidelities to be reproducibly achieved. In the near future, absolute placement accuracy appears feasible through the development of STM methods such as tip-assisted incorporation [51,52]. Assuming absolute

atomic precision of qubit fabrication, the 2P-3P becomes very attractive as it promises ΔE as high as 891 MHz and the CNOT error as low as 0.024%.

VIII. IMPACT OF CHARGE NOISE AND MAGNETIC NOISE ON THE CNOT GATE FIDELITY

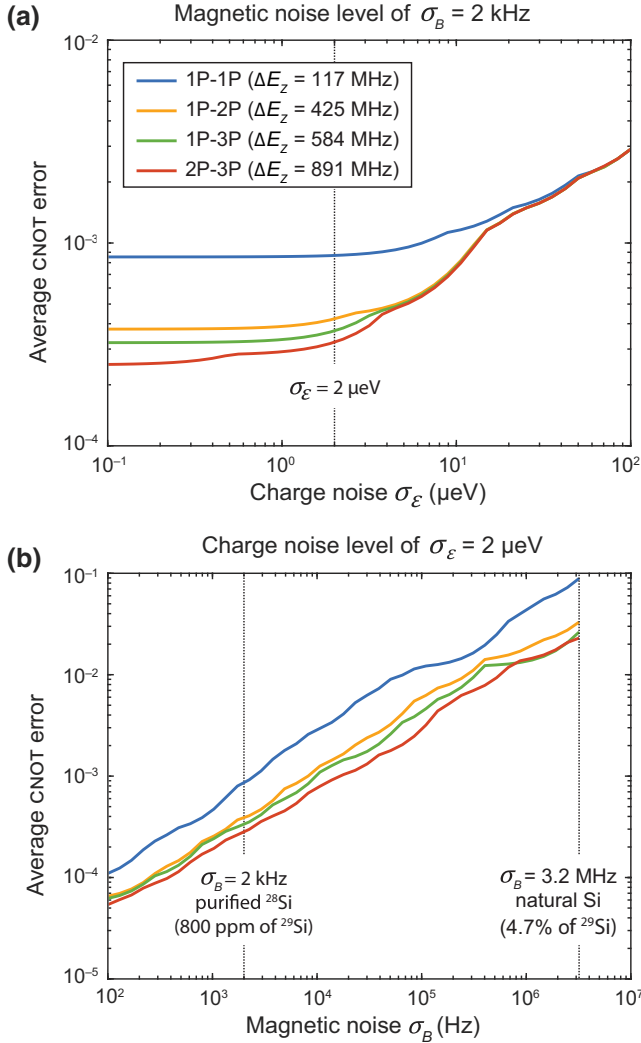In the previous section we show that the two-qubit CNOT gate fidelity benefits from the large ΔE values offered by

(a) Magnetic noise level of σ_B = 2 kHz

- 1P-1P (ΔE_z = 117 MHz)
- 1P-2P (ΔE_z = 425 MHz)
- 1P-3P (ΔE_z = 584 MHz)
- 2P-3P (ΔE_z = 891 MHz)

$\sigma_{\mathcal{E}}$ = 2 µeV

Average CNOT error vs Charge noise $\sigma_{\mathcal{E}}$ (µeV)

(b) Charge noise level of $\sigma_{\mathcal{E}}$ = 2 µeV

σ_B = 2 kHz purified ^{28}Si (800 ppm of ^{29}Si)

σ_B = 3.2 MHz natural Si (4.7% of ^{29}Si)

Average CNOT error vs Magnetic noise σ_B (Hz)

FIG. 5. Impact of noise on the CNOT gate fidelity. (a) The average CNOT error as a function of charge-noise level σ_ϵ, calculated for a fixed gate time of $T_{\text{CNOT}} = 2$ µs and the magnetic noise of $\sigma_B = 2$ kHz corresponding to the purified silicon-28 (800 ppm). Line traces represent the highest achievable values using different donor numbers. Larger donor dots outperform 1P-1P, particularly for low charge-noise levels. (b) The average CNOT error as a function of magnetic noise level σ_B. Calculations are performed for the charge-noise level of $\sigma_\epsilon = 2$ µeV, indicated with a purple vertical line in (a). As expected, for all donor numbers the CNOT gate is highly susceptible to the Overhauser noise produced by the ^{29}Si nuclear spins.

multidonor qubits. All of the above results assume the charge-noise level of $\sigma_\epsilon = 2$ µeV and the magnetic noise level of $\sigma_B = 2$ kHz. We now vary the standard deviation of detuning noise σ_ϵ and the magnetic noise σ_B and investigate the impact of noise levels on the CNOT gate fidelity.

In Fig. 5(a) we show the average CNOT gate error, achievable with 1P-1P, 1P-2P, 1P-3P, and 2P-3P qubit pairs, as a function of charge noise σ_ϵ, for a fixed magnetic noise of $\sigma_B = 2$ kHz. For each qubit pair, we assume the best-case atomic arrangement, that is the arrangement corresponding to the the highest ΔE. As expected, we observe a reduction in the gate error for lower charge noise and larger ΔE values. We note that all calculations assume a tunnel coupling of $t_c = 4$ GHz between the qubits. The impact of charge noise can be mitigated by increasing the t_c, which would effectively lower the fluctuations in J, $\sigma_J = \sigma_\epsilon \partial J / \partial \epsilon$, for a given σ_ϵ value [12]. However, with the t_c being too large it might be challenging to turn J completely off ($J \ll \Delta E$), as needed for independent spin control and measurements, since this will then require a large amplitude of the detuning pulse. The optimal tunnel coupling depends therefore on available detuning voltage range, which can be limited either by device leakage or by pulse amplitude of the control instrumentation. In practice, the most optimal set of experimental parameters used for a CNOT gate needs to be tailored for a specific device.

Next, we investigate the sensitivity of the CNOT gate on the magnetic noise originating from the ^{29}Si nuclear spins. In Fig. 5(b) we plot the average CNOT gate error for a fixed charge-noise level ($\sigma_\epsilon = 2$ µeV) while varying the magnetic noise level from $\sigma_B = 100$ Hz to 3.2 MHz. The magnetic noise levels corresponding to natural silicon and purified silicon-28 (800 ppm of ^{29}Si) are indicated with vertical purple lines. As expected, we find that, regardless of donor numbers, the average CNOT error can be largely suppressed using isotopic purification of silicon-28. In particular, for the purification level of 800 ppm ^{29}Si, the CNOT error rates can be brought below 0.03% when using multidonor dots and approximately 0.1% for single donors. This is a significant result as it confirms the benefit of using atomically engineered hyperfine fields on the two-qubit CNOT gate fidelity.

IX. DISCUSSION AND SUMMARY

In summary, we develop a theoretical framework that allows us to calculate the CNOT gate fidelity between two electron spins hosted on multidonor qubits. We find that, with realistic noise levels, multidonor qubits (such as 2P-3P) allow for the CNOT fidelities as high as 99.98%, compared to only $\sim 99.9\%$ achievable with single donors (1P-1P). This improvement in the CNOT fidelity is attributed to the fact that we can engineer large hyperfine couplings in multidonor dot qubits leading to a large magnitude for

ΔE when the P nuclear states on both qubits are initialized in opposite directions. We use a theoretical model of the two-qubit CNOT gate to optimize both the fabrication *and* measurement stages of the experiment. Firstly, our results suggest that to optimize the CNOT gate fidelity, the number of donors and their atomic arrangement within the qubits need to be engineered at the atomic level during the STM lithography stage to achieve large A values. Secondly, once the device is fabricated, the model allows us to calculate the optimal qubit control parameters that yield the highest achievable CNOT gate fidelity. More specifically, if the A, t_c, T_2^*, and σ_ϵ parameters are known, the model determines the optimal amplitude of the J pulse (optimal ϵ), optimal frequency of the ESR pulse (optimal $f_\uparrow^L$) and optimal power of the ESR pulse (optimal T_{CNOT}). Our model provides a comprehensive guide to recognizing and mitigating limiting factors in the CNOT gate to create a roadmap for high-fidelity two-qubit gates in donor-based systems.

CONFLICT OF INTEREST

M.Y.S. is a director of the company Silicon Quantum Computing Pty Ltd.

APPENDIX: ERROR SOURCES FOR A TWO-QUBIT CROT GATE

It is useful to realize that the CNOT gate fidelity can be limited by several different mechanisms. To understand the limitations of the CNOT gate fidelity, we divide the sources of error into five main categories:

1. Unwanted driving of the target qubit when the control qubit is in a $|\downarrow\rangle$ state.

This error is associated with large negative ϵ values for which the target qubit ESR frequencies $f_\downarrow^L$ and $f_\uparrow^L$ are not well separated. This error can be reduced by increasing J.

2. Unwanted driving of the control qubit.

The ideal CNOT gate assumes that the control qubit remains unchanged during the gate operation. However, at detuning values approaching zero, the resonant frequencies of both qubits converge (branches $f_\uparrow^L$ and $f_\downarrow^R$). Thus, when applying an ESR pulse to perform a rotation of the target qubit, the control qubit might be inadvertently flipped. This error can be reduced by decreasing J.

3. Deviation from the computational basis.

After the CNOT operation, both electron spins are measured, which corresponds to the projection from the $\{\downarrow\downarrow, \widetilde{\downarrow\uparrow}, \widetilde{\uparrow\downarrow}, \uparrow\uparrow\}$ basis onto the computational basis $\{\downarrow\downarrow, \downarrow\uparrow, \uparrow\downarrow, \uparrow\uparrow\}$. As a result of the projective readout, there is a finite probability that the spins will be incorrectly mapped back onto the computational basis. For example, the $|\widetilde{\downarrow\uparrow}\rangle$ state can be incorrectly projected into the $|\uparrow\downarrow\rangle$ state, which manifests itself as an error in the CNOT gate [19]. This error is proportional to the angle $\theta = \arctan(J/\Delta E)$. When projected onto the measurement axis, the visibility of the target qubit Rabi oscillations is reduced and can be written as

$$V_{\text{Rabi}} = \frac{\Delta E^2}{\Delta E^2 + J^2}. \qquad (A1)$$

This error can be reduced by decreasing J (by decreasing ϵ) and/or increasing ΔE. It should be noted that this error can be avoided by slowly ramping the detuning such that the two-spin states are adiabatically mapped from the hybridized basis to the computational basis. The slow ramps, however, extend the duty cycle of the two-qubit gate adding an overhead to the operation of the quantum processor. While in this work we consider square-shaped detuning pulses to maximize the gate speed, in future work different pulse shapes can be considered to find a desired trade-off between speed and fidelity of two-qubit gates.

4. T_2^* dephasing process.

Due to fluctuating of the surrounding nuclear spin bath, the amplitude of Rabi oscillations decay over time and limits the CNOT gate fidelity. This error can be reduced by shortening the gate time T_{CNOT}, or extending T_2^* with silicon purification methods that remove spinful ^{29}Si nuclei [30,53].

5. Charge noise.

The fluctuations in detuning (ϵ) result in the target qubit being detuned from its resonance, hence the Rabi frequency of the target qubit varies throughout the CNOT gate and leads to dephasing. This error can be reduced by decreasing ϵ, since charge noise has been shown to be proportional to $\partial J/\partial \epsilon$. The impact of charge noise can be also reduced by shortening the two-qubit gate time.

Our numerical model includes the combined effect of all the above-mentioned error sources. This is in contrast to previous models [22] that have simply considered and added individual errors. We also note that the competition between the different error sources results in an optimal detuning ϵ as well as optimal ESR frequency, which can be determined using our model to maximize CNOT gate fidelity.

[1] Bruce E. Kane, A silicon-based nuclear spin quantum computer, Nature 393, 133 (1998).

[2] B. Koiller, X. Hu, and S. Das Sarma, Exchange in Silicon-Based Quantum Computer Architecture, Phys. Rev. Lett. 88, 027903 (2002).

[3] C. J. Wellard, L. C. L. Hollenberg, F. Parisoli, L. M. Kettle, H.-S. Goan, J. A. L. McIntosh, and D. N. Jamieson, Electron exchange coupling for single-donor solid-state spin qubits, Phys. Rev. B 68, 195209 (2003).

[4] N. T. Gamble, J. K. Jacobson, E. Nielsen, A. D. Baczewski, J. E. Moussa, I. Montaño, and R. P. Muller, Multivalley effective mass theory simulation of donors in silicon, Phys. Rev. B 91, 235318 (2015).

[5] Y. He, S. K. Gorman, D. Keith, L. Kranz, J. G. Keizer, and M. Y. Simmons, A two-qubit gate between phosphorus donor electrons in silicon, Nature 571, 371 (2019).

[6] M. Fuechsle, J. A. Miwa, S. Mahapatra, H. Ryu, S. Lee, O. Warschkow, L. C. L. Hollenberg, G. Klimeck, and M. Y. Simmons, A single-atom transistor, Nat. Nanotechnol. 7, 242 (2012).

[7] T. F. Watson, B. Weber, Y. L. Hsueh, L. C. Hollenberg, R. Rahman, and M. Y. Simmons, Atomically engineered electron spin lifetimes of 30 s in silicon, Sci. Adv. 3, e1602811 (2017).

[8] J. P. Dehollain, J. T. Muhonen, R. Blume-Kohout, K. M. Rudinger, J. K. Gamble, E. Nielsen, A. Laucht, S. Simmons, R. Kalra, and A. S. Dzurak, et al., Optimization of a solid-state electron spin qubit using gate set tomography, New J. Phys. 18, 103018 (2016).

[9] M. T. Madzik, A. Laucht, F. E. Hudson, A. M. Jakob, B. C. Johnson, D. N. Jamieson, K. M. Itoh, A. S. Dzurak, and A. Morello, Conditional quantum operation of two exchange-coupled single-donor spin qubits in a MOS-compatible silicon device, Nat. Commun. 12, 1 (2021).

[10] C. D. Hill, E. Peretz, S. J. Hile, M. G. House, M. Fuechsle, S. Rogge, M. Y. Simmons, and L. C. L. Hollenberg, A surface code quantum computer in silicon, Sci. Adv. 1, e1500707 (2015).

[11] K. C. Nowack, M. Shafiei, M. Laforest, G. E. D. K. Prawiroatmodjo, L. R. Schreiber, C. Reichl, W. Wegscheider, and L. M. K. Vandersypen, Single-shot correlations and two-qubit gate of solid-state spins, Science 333, 1269 (2011).

[12] O. E. Dial, M. D. Shulman, S. P. Harvey, H. Bluhm, V. Umansky, and A. Yacoby, Charge Noise Spectroscopy using Coherent Exchange Oscillations in a Singlet-Triplet Qubit, Phys. Rev. Lett. 110, 146804 (2013).

[13] M. Veldhorst, C. H. Yang, J. C. C. Hwang, W. Huang, J. P. Dehollain, J. T. Muhonen, S. Simmons, A. Laucht, F. E. Hudson, K. M. Itoh, A. Morello, and A. S. Dzurak, A two-qubit logic gate in silicon, Nature 526, 410 (2015).

[14] T. F. Watson, S. G. J. Philips, E. Kawakami, D. R. Ward, P. Scarlino, M. Veldhorst, D. E. Savage, M. G. Lagally, M. Friesen, S. N. Coppersmith, M. A. Eriksson, and L. M. K. Vandersypen, A programmable two-qubit quantum processor in silicon, Nature 555, 633 (2018).

[15] X. Xue, T. F. Watson, J. Helsen, D. R. Ward, D. E. Savage, M. G. Lagally, S. N. Coppersmith, M. A. Eriksson, S. Wehner, and L. M. K. Vandersypen, Benchmarking Gate Fidelities in a Si/SiGe Two-Qubit Device, Phys. Rev. X 9, 021011 (2019).

[16] X. Xue, M. Russ, N. Samkharadze, B. Undseth, A. Sammak, G. Scappucci, and L. M. K. Vandersypen, Quantum logic with spin qubits crossing the surface code threshold, Nature 601, 343 (2022).

[17] A. G. Fowler, M. Mariantoni, J. M. Martinis, and A. N. Cleland, Surface codes: Towards practical large-scale quantum computation, Phys. Rev. A 86, 032324 (2012).

[18] W. Huang, C. H. Yang, K. W. Chan, T. Tanttu, B. Hensen, R. C. C. Leon, M. A. Fogarty, J. C. C. Hwang, F. E. Hudson, K. M. Itoh, A. Morello, A. Laucht, and A. S. Dzurak, Fidelity benchmarks for two-qubit gates in silicon, Nature 569, 532 (2019).

[19] D. M. Zajac, A. J. Sigillito, M. Russ, F. Borjans, J. M. Taylor, G. Burkard, and J. R. Petta, Resonantly driven CNOT gate for electron spins, Science 359, 439 (2018).

[20] A. Noiri, K. Takeda, T. Nakajima, T. Kobayashi, A. Sammak, G. Scappucci, and S. Tarucha, Fast universal quantum gate above the fault-tolerance threshold in silicon, Nature 601, 338 (2022).

[21] X. Wu, D. R. Ward, J. R. Prance, D. Kim, J. K. Gamble, R. T. Mohr, Z. Shi, D. E. Savage, M. G. Lagally, M. Friesen, S. N. Coppersmith, and M. A. Eriksson, Two-axis control of a singlet–triplet qubit with an integrated micromagnet, Proc. Nat. Acad. Sci. 111, 11938 (2014).

[22] R. Kalra, A. Laucht, C. D. Hill, and A. Morello, Robust Two-Qubit Gates for Donors in Silicon Controlled by Hyperfine Interactions, Phys. Rev. X 4, 021044 (2014).

[23] N. I. Dumoulin Stuyck, F. A. Mohiyaddin, R. Li, M. Heyns, B. Govoreanu, and I. P. Radu, Low dephasing and robust micromagnet designs for silicon spin qubits, Appl. Phys. Lett. 119, 094001 (2021).

[24] L. Kranz, S. K. Gorman, B. Thorgrimsson, Y. He, D. Keith, J. G. Keizer, and M. Y. Simmons, Exploiting a single-crystal environment to minimize the charge noise on qubits in silicon, Adv. Mater. 32, 2003361 (2020).

[25] D. Keith, S. K. Gorman, Y. He, L. Kranz, and M. Y. Simmons, Impact of charge noise on electron exchange interactions in semiconductors, npj Quantum Inf. 8, 1 (2022).

[26] M. Veldhorst, J. C. C. Hwang, C. H. Yang, A. W. Leenstra, B. de Ronde, J. P. Dehollain, J. T. Muhonen, F. E. Hudson, K. M. Itoh, A. Morello, and A. S. Dzurak, An addressable quantum dot qubit with fault-tolerant control-fidelity, Nat. Nanotechnol. 9, 981 (2014).

[27] Y. Wang, C.-Y. Chen, G. Klimeck, M. Y. Simmons, and R. Rahman, Characterizing Si:P quantum dot qubits with spin resonance techniques, Sci. Rep. 6, 31830 (2016).

[28] S. J. Hile, L. Fricke, M. G. House, E. Peretz, C. Y. Chen, Y. Wang, M. Broome, S. K. Gorman, J. G. Keizer, R. Rahman, and M. Y. Simmons, Addressable electron spin resonance using donors and donor molecules in silicon, Sci. Adv. 4, 00 (2018).

[29] J. J. Pla, K. Y. Tan, J. P. Dehollain, W. H. Lim, J. J. L. Morton, F. A. Zwanenburg, D. N. Jamieson, A. S. Dzurak, and A. Morello, High-fidelity readout and control of a nuclear spin qubit in silicon, Nature 496, 334 (2013).

[30] J. T. Muhonen, J. P. Dehollain, A. Laucht, F. E. Hudson, R. Kalra, T. Sekiguchi, K. M. Itoh, D. N. Jamieson, J. C.

McCallum, A. S. Dzurak, and A. Morello, Storing quantum information for 30 seconds in a nanoelectronic device, Nat. Nanotechnol. **9**, 986 (2014).

[31] M. T. Madzik, S. Asaad, A. Youssry, B. Joecker, K. M. Rudinger, E. Nielsen, K. C. Young, T. J. Proctor, A. D. Baczewski, and A. Laucht, *et al.*, Precision tomography of a three-qubit donor quantum processor in silicon, Nature **601**, 348 (2022).

[32] J. J. Pla, K. Y. Tan, J. P. Dehollain, W. H. Lim, J. J. L. Morton, D. N. Jamieson, A. S. Dzurak, and A. Morello, A single-atom electron spin qubit in silicon, Nature **489**, 541 (2012).

[33] M. A. Broome, S. K. Gorman, M. G. House, S. J. Hile, J. G. Keizer, D. Keith, C. D. Hill, T. F. Watson, W. J. Baker, L. C. L. Hollenberg, and M. Y. Simmons, Two-electron spin correlations in precision placed donors in silicon, Nat. Commun. **9**, 980 (2018).

[34] B. Hensen, W. W. Huang, C.-H. Yang, K. W. Chan, J. Yoneda, T. Tanttu, F. E. Hudson, A. Laucht, K. M. Itoh, and T. D. Ladd, *et al.*, A silicon quantum-dot-coupled nuclear spin qubit, Nat. Nanotechnol. **15**, 13 (2020).

[35] T. Meunier, V. E. Calado, and L. M. K. Vandersypen, Efficient controlled-phase gate for single-spin qubits in quantum dots, Phys. Rev. B **83**, 121403 (2011).

[36] G. Feher, Electron spin resonance experiments on donors in silicon. I. electronic structure of donors by the electron nuclear double resonance technique, Phys. Rev. **114**, 1219 (1959).

[37] M. A. Fogarty, K. W. Chan, B. Hensen, W. Huang, T. Tanttu, C. H. Yang, A. Laucht, M. Veldhorst, F. E. Hudson, K. M. Itoh, D. Culcer, T. D. Ladd, A. Morello, and A. S. Dzurak, Integrated silicon qubit platform with single-spin addressability, exchange control and single-shot singlet-triplet readout, Nat. Commun. **9**, 4370 (2018).

[38] Guido Burkard, Quantum computation and communication using electron spins in quantum dots and wires. PhD thesis, University of Basel, 2001.

[39] Guido Burkard, Daniel Loss, and David P. DiVincenzo, Coupled quantum dots as quantum gates, Phys. Rev. B **59**, 2070 (1999).

[40] X. Wu, D. R. Ward, J. R. Prance, D. Kim, J. K. Gamble, R. T. Mohr, Z. Shi, D. E. Savage, M. G. Lagally, M. Friesen, S. N. Coppersmith, and M. A. Eriksson, Two-axis control of a singlet–triplet qubit with an integrated micromagnet, Proc. Nat. Acad. Sci. **111**, 11938 (2014).

[41] J. L. O'Brien, G. J. Pryde, A. Gilchrist, D. F. V. James, N. K. Langford, T. C. Ralph, and A. G. White, Quantum Process Tomography of a Controlled-NOT Gate, Phys. Rev. Lett. **93**, 080502 (2004).

[42] M. Russ, D. M. Zajac, A. J. Sigillito, F. Borjans, J. M. Taylor, J. R. Petta, and G. Burkard, High-fidelity quantum gates in Si/SiGe double quantum dots, Phys. Rev. B **97**, 085421 (2018).

[43] Luc Devroye, in Proceedings of the 18th conference on Winter simulation, p. 260, 1986.

[44] R. M. Jock, N. T. Jacobson, P. Harvey-Collard, A. M. Mounce, V. Srinivasa, D. R. Ward, J. Anderson, R. Manginell, J. R. Wendt, M. Rudolph, T. Pluym, J. K. Gamble, A. D. Baczewski, W. M. Witzel, and S. M. Carroll, A silicon metal-oxide-semiconductor electron spin-orbit qubit, Nat. Commun. **9**, 1768 (2018).

[45] J. T. Muhonen, A. Laucht, S. Simmons, J. P. Dehollain, R. Kalra, F. E. Hudson, S. Freer, K. M. Itoh, D. N. Jamieson, and J. C. McCallum, *et al.*, Quantifying the quantum gate fidelity of single-atom spin qubits in silicon by randomized benchmarking, J. Phys.: Condens. Matter **27**, 154205 (2015).

[46] Y. Wang, A. Tankasala, L. C. L. Hollenberg, G. Klimeck, M. Y. Simmons, and R. Rahman, Highly tunable exchange in donor qubits in silicon, npj Quantum Inf. **2**, 16008 (2016).

[47] R. Rahman, C. J. Wellard, F. R. Bradbury, M. Prada, J. H. Cole, G. Klimeck, and L. C. L. Hollenberg, High Precision Quantum Control of Single Donor Spins in Silicon, Phys. Rev. Lett. **99**, 036403 (2007).

[48] H. Buch, S. Mahapatra, R. Rahman, A. Morello, and M. Y. Simmons, Spin readout and addressability of phosphorous-donor clusters in silicon, Nat. Commun. **4**, 2017 (2013).

[49] A. Laucht, J. T. Muhonen, F. A. Mohiyaddin, R. Kalra, J. P. Dehollain, S. Freer, F. E. Hudson, M. Veldhorst, R. Raman, G. Kilmeck, K. M. Itoh, D. N. Jamieson, J. C. McCallum, A. S. Dzurak, and A. Morello, Electrically controlling single-spin qubits in a continuous microwave field, Sci. Adv. **1**, e1500022 (2015).

[50] The ranges of hyperfine couplings that can be achieved with different donor numbers include unpublished atomistic tight-binding calculations by Rajib Rahman and MD Serajum Monir.

[51] J. H. G. Owen, E. Fuchs, J. N. Randall, and J. R. Von Ehr, 2D dopant arrays using a tip-assisted incorporation process. https://www.zyvexlabs.com/wp-content/uploads/2016/12/Abstract_MNE2018_JHGOv2.pdf, 2018. Online; accessed 10 August 2020.

[52] Q. Liu, Y. Lei, X. Shao, F.i Ming, H. Xu, X. Wang, and K.and Xiao, Controllable dissociations of PH_3 molecules on Si (001), Nanotechnology **27**, 135704 (2016).

[53] E. J. Connors, J. J. Nelson, H. Qiao, L. F. Edge, and J. M. Nichol, Low-frequency charge noise in Si/SiGe quantum dots, Phys. Rev. B **100**, 165305 (2019).